# Structural Performance of the Esfahan Shah Mosque

Ali T. Dinani, Ph.D.[1]; Giacomo Destro Bisol[2]; Javier Ortega, Ph.D.[3]; and Paulo B. Lourenço, Ph.D.[4]

**Abstract:** Structural assessment and seismic vulnerability of ancient masonry buildings is a difficult task even when employing advanced specialized technical skills, which requires a complex study. This paper aims to assess the structural and seismic safety of the Esfahan Shah Mosque in Iran by numerically investigating the nonlinear behavior of the mosque for different scenarios and identify if there is a correlation between crack patterns resulting from numerical analysis, inspection and historical evidence. Firstly, the numerical model of mosque is developed and updated using the experimental parameters obtained from a non-destructive test (NDT) campaign that included ambient vibration and sonic testing. Secondly, the FE calibrated model is used to evaluate the structural behavior of the mosque under vertical loading, including the influence of the soil and a sensitivity analysis varying the masonry material properties. Besides, the paper discusses the structural behavior

[1] Postdoctoral Researcher, Department of Architecture, Built environment and Construction engineering (ABC), Polytechnic of Milan, Piazza Leonardo da Vinci 32, 20133 Milan, Italy (corresponding author). Email: alitavakoli.dinani@polimi.it

[2] M.Sc., Ph.D. candidate, Department of Structural and Geotechnical Engineering, Sapienza University of Rome, Via Eudossiana 18, 00184 Rome, Italy. Email: giacomo.destrobisol@uniroma1.it

[3] Postdoctoral Researcher, Department of Civil Engineering, ISISE, University of Minho, Guimarães, Campus de Azurém, 4800-058 Guimarães, Portugal. Email: javier.ortega@civil.uminho.pt

[4] Professor, Department of Civil Engineering, ISISE, University of Minho, Guimarães, Campus de Azurém, 4800-058 Guimarães, Portugal. Email: pbl@civil.uminho.pt

Note. This manuscript was submitted on July 28, 2020; approved on April 19, 2021; published online on July 31, 2021. This paper is part of the Journal of Structural Engineering, © 2021 American Society of Civil Engineers, ISSN 0733-9445.

**DOI: 10.1061/(ASCE)ST.1943-541X.0003108**.

The abstract link in ASCE library: https://ascelibrary.org/doi/abs/10.1061/%28ASCE%29ST.1943-541X.0003108

of radial stiffening walls that connect the inner and outer domes of the mosque. Finally, pushover analysis was carried out to assess the seismic safety of the building and the efficiency of the structural strengthening implemented in the early 20th century. The different technical observations and analyses lead to better understanding the double dome and the *eyvan* (a rectangular space, usually vaulted, walled on three sides, with one end entirely open) as the most vulnerable parts of the structure, which validates the structural strengthening of the 1930s. Yet, improving the connection between the stiffening walls and the two domes could effectively increase the global structural performance of the building.

**Keywords:** Masonry structures; Non-destructive testing, Numerical modeling; Sensitivity analysis; Esfahan Shah Mosque; Seismic safety assessment

## INTRODUCTION

Studies oriented to conservation and restoration of historical structures adopt structural analysis as a way to better understand the genuine structural features of the building, to characterize its present condition and to determine the structural safety for a variety of actions such as gravity, soil settlements and lateral capacity under seismic loading (Roca et al. 2010). Structural analysis is an indispensable tool to provide a reliable safety evaluation, which needs a validated and calibrated numerical model (ICOMOS/ISCARSAH 2005). Using the most advanced computational tools available for structural assessment is common due to the complexity of historical monuments. Yet, performing numerical analysis in unique historic buildings such as the Esfahan's Shah Mosque, in Iran, demands the consideration of different scenarios due to the complexity of the structure, and the uncertainty in the definition such as soil characteristics, boundary conditions, construction details or material properties. Therefore, any structural analysis should try to incorporate qualitative measures based on historical research and onsite observations and inspections.

Substantially, in situ experimental campaigns are a principal complementary task to numerical modeling and structural analysis. In case of historical masonry, since the structure cannot be excessively damaged, in situ non-destructive testing (NDT) can provide an indirect evaluation of materials properties (Binda et al. 2000) and is highly recommended. This work provides an experimental in situ campaign of NDT including dynamic identification and sonic tests. The sonic test characterizes the elastic properties of the material and the dynamic characterization test allows to obtain the dynamic properties of a structure in terms of natural frequencies and vibration modes. The latter leads to a better understanding of the global behavior of existing structures and can be used to calibrate the numerical model, while the formal gives only local values, at the location of measurement.

Therefore, the objective of the current article is to study the structural performance and assess the seismic safety of the Shah Mosque, a UNESCO World Heritage Site since 1979, through an integrated methodology combining Finite Element (FE) analysis and experimental NDT. Following the recent historiography of building technology, FE modeling and structural analysis of the hybrid double dome (HDD) (Dinani et al. 2019; Dinani 2019), this work expands the analysis to the area where the HDD is placed, considering the effect of adjacent structures. The paper presents the continuation of the most recent structural modeling works (Destro Bisol 2019), using an updated model that includes the structural intervention of the early 20th century.

Following the validation and calibration of the FE model through the experimental results derived from in situ NDT, the nonlinear analyses carried out under vertical and seismic loads take into account different scenarios to explore not merely the structural performance of the Shah Mosque, but also to discuss: (a) the influence of the HDD's stiffening walls on the global behavior; (b) the structural response of the dome in the strengthened condition; and (c) the influence of the soil. Simultaneously, a sensitivity analysis is performed to investigate the importance of the masonry tensile behavior on the structural response. In the following, the correlation between the crack patterns obtained from the numerical analysis and existing damages was discussed. Afterwards, the seismic safety assessment of the Shah Mosque is presented.

## STRUCTURAL FEATURES

The Safavid (dynasty ruling Persia from 1501 to 1722) chronicles report the initial efforts for urban development of Esfahan as Safavid capital in late 16$^{th}$ century, in which the work on the Shah Mosque began on the southern edge of the Naghsh-e Jahan Meidan to rearrange the city's traffic pattern to bring more clientele into the new market area of Meidan (Monshi 2003; Hosseini Jonabadi 2000). The construction of the Shah Mosque started on 7$^{th}$ May 1611 and was completed in 1636 along with a number of other Safavid projects. The mosque is a lofty structure that adopts a glazed bulbous double dome as a hybrid structure and incorporates four-eyvan patterns that face each other across a central courtyard with an overall dimension of 145 m in length and 140 m in width (Fig. 1 and Fig. 2 (a)).

The HDD of the mosque is a composite structure of brick double dome with radial stiffener walls, wooden ties, and struts with different configurations adopted in the building construction and the structural system (Dinani et al. 2019). The HDD stands on a square base of 22.5 m with almost 50 m height (with almost 11 m height of space in-between, see Fig. 1(b)**)** and the outer bulbous dome is on 32 radial stiffening walls (*khashkhashi*) and a so-called drum (*geriv)*, raised 7 m high from the springing point of the inner pointed dome. One of the structural challenges of the masonry bulbous double domes is that the thrust line cannot follow the geometric line of the bulbous dome, as the tangent to this line at the springing of the profile cannot exceed the vertical line (Croci 1998). Thus, the equilibrium state of the Shah Mosque's masonry bulbous dome is impossible to ensure without stiffeners retaining the horizontal thrust. A system of diagonal and encircling wooden ties system plays an indispensable role in the construction process and may be also beneficial in improving the connections of the masonry elements (inner dome, outer dome and stiffeners), meanwhile, supports the horizontal thrusts prevention of the bulbous dome (Dinani 2019).

The Southern eyvan, next to the HDD, dimensions are extraordinary with the inner height of 26.7 m and a pointed semi-dome vault span of 18.3 m, erected on thick walls (4.5 m to 6.5 m). Although a half-dome can freely stand (Heyman 1995), and can be stable subjected to horizontal and/or vertical reactions that resist overturning, it is fragile and, in the case of Shah Mosque, faced with the danger of collapse according to (Salnameh-e Maaret-e Esfahan, Sal-e Tahsili 1313-1314 1935). In addition, two minarets with a height of 45.0 m, stand on both sides of the eyvan's outer arch and help to provide resistance to the arch's horizontal thrust by the self-weight. However, these minarets are likely to make the structure less resistant to seismic action due to lateral forces developed.

There have been several restorations in the Shah Mosque, mostly repairing ceramic tiles from time to time and partially structural interventions. Major works undertaken during the 1930s and 2011 to 2021 have contributed to repair ceramic tiles and a vital structural strengthening was implemented in the 1930s. Earlier evidence refers to the 1844 earthquake, when the south Eyvan's cracks were repaired superficially (Varjavand 1976). In 1932, in danger of collapse, the eyvan was leaning outwards, which asked for a structural intervention.

The outer dome exhibits several cracks visible from the in-between space of the domes. Vertical cracks in the intersection of the outer dome and stiffening walls (Fig. 3 (c)) are seen on the intrados and underneath the tile layer on the outer dome's extrados. These cracks were seemingly caused by the horizontal thrust of the bulbous dome and the weakness of the connections that asked for the encircling ties system strengthening in the 1940s (Fig 2 (b),(c)). The cracks also are visible in the semi-dome of the eyvan (Fig. 3(a) and 15(a)) as well as major vertical cracks in two flank walls where the semi dome is seated on (Fig. 3b).

The crack finally continues in the staircase towards the ground floor (Dinani et al. 2019; Dinani 2019).

Hossein Moarefi (1893-1976), a maestro in restoration, proposed an ingenious solution to constrain the distribution of the cracks of eyvan and HDD by a net of I-beam (Fig. 3 (a)) and cable system along with foundation strengthening in 1932 (Varjavand 1976; Salnameh-e Maaret-e Esfahan, Sal-e Tahsili 1313-1314 1935; Akhgar 1936). Later in 1940s, he applied an encircling steel ties system around the bulbous dome in the position of the traditional encircling wooden ties system, with 90 m length (Fig. 2(b)) (Akhgar 1941). Another steel profile ring has been applying on the extrados of the outer dome from 2011 to 2021, even if its necessity and consequences should be discussed and monitored (Fig. 2 (c)).

## IN SITU TESTING AND FINITE ELEMENT MODEL DEFINITION

### *Material identification and inelastic behavior*

The macro modeling strategy is usually adopted for masonry modeling in large structures, in which units and joints are modeled as a homogeneous continuum (Lourenco 1996). Following this premise, the material properties of masonry are determined here based on: (a) non-destructive sonic tests that have been carried out on site on the Shah Mosque, which allowed estimating elastic properties, namely Young's modulus and Poisson's ratio; and (b) literature review to estimate the remaining nonlinear properties.

Sonic tests are indisputably the most applied non-destructive investigation technique to characterize the elastic properties of historic masonry structures (Binda et al. 2007; Binda et al. 2009). They allow estimating masonry elastic properties because of the relationship between the sonic wave velocity propagating through the material and its elastic mechanical properties (Everett 2013). The validity of the test has been widely demonstrated through on-site and laboratory works (Miranda et al. 2012; Miranda et al. 2016; Maccarini et al. 2019; Murano et al. 2019; Sánchez-Aparicio et al. 2019). Even if specific standards to follow for sonic tests on masonry structures do not exist, the procedure is based on the same physical principles as the ultrasonic pulse velocity method developed for testing concrete, which adopts a procedure well-established by international standards (ASTM C597-09 2009; CEN12504-04 2004). It is stressed that ultrasonic tests are usually not applicable to masonry due to the low energy used and the physical characteristics of the material. The velocity of an elastic wave propagating through a solid material like masonry is related to the density, Young's modulus, and Poisson's ratio of the material through the following expressions:

$$V_P = \sqrt{\frac{E(1-\nu)}{\rho(1+\nu)(1-2\nu)}} \tag{1}$$

$$V_R = \frac{0.87+1.12\nu}{1+\nu} \cdot \sqrt{\frac{E}{\rho} \cdot \frac{1}{2(1+\nu)}} \tag{2}$$

and the combination of Eq. (1) and (2), gives:

$$\frac{V_P}{V_R} = \sqrt{\frac{2(1-\nu)}{(1-2\nu)} \cdot \frac{(1+\nu)^2}{(0.87+1.12\nu)^2}} \tag{3}$$

where $V_P$ and $V_R$ are, P-wave velocity and R-wave velocity respectively; E is the Young's modulus; $\nu$ is the Poisson's ratio; and $\rho$ is the mass density. Nevertheless, it is noted that these expressions were developed for homogeneous, elastic, isotropic and semi-infinite materials, which typically does not apply to masonry. Therefore, for historical masonry, results have to be interpreted carefully, acknowledging that they are an estimation of the mechanical properties (Berra et al. 1992; Binda et al. 2001).

Due to the site conditions, indirect (i.e. on a single surface) sonic testing was carried out on-site in June 2019, with a configuration where the emitter (instrumented hammer) and receiver (accelerometer) are placed on the same side of the wall. In this setting, both longitudinal or P-waves and surface or R-waves can be obtained (Miranda et al. 2012). Indirect sonic tests were performed at different parts of the double dome and the eyvan (Fig. 4(a)). Table 1 presents the results obtained at the selected points, in which the mass density was assumed as 1800 kg/m$^3$, as proposed by NTC 2018 for brick masonry (NTC 2018; Circular n° 7 of NTC2018 2019). The equipment used included an instrumented hammer (PCB Model 086D05) with a measurement range of ±22240 N, as an active source for wave generation and an accelerometer (PCB model 352B) with a measurement range of ±5 g pk and sensitivity of (±5%) 1000 mV/g, for the wave reception along with a LabView module to visualize the transmitted and received signals in the time domain. In the operation condition, a grid of test points was marked with a distance of 0.75 m between the transmitter and receiver, except for the largest stiffener walls where the distance was taken as 1 m. Then, impacting the hammer 10 times on the marked point generated sonic elastic waves that were received on an accelerometer positioned on the neighboring grid point.

The investigated structure of building is made of brick masonry with the same constituents underneath the thin layer of local marble plaque and ceramic tiles. The elastic masonry mechanical properties finally adopted for the FE model are presented in Table 2. In this regard, an average Poisson's ratio of 0.36 was obtained from the sonic tests, which is considered high with respect to typical values for masonry, typically ranging between 0.2 and 0.30 (Miranda et al. 2012). Nevertheless, in the absence of other source of information, the data gathered in-situ through the tests was used for the numerical model. As Miranda et al. (2015) pointed out, the variability of the Poisson's ratio does not introduce major differences on the elasticity modulus calculated using equations (1) and (2). Moreover, the likely overestimation of the Poisson's ratio considered has a minor influence in the structural analysis, as the value changes during the inelastic process. The achieved Young's modulus of 1050 MPa is close to the minimum value of 1200 MPa, considering a reduction coefficient of 0.8 for the bed joint greater than 13 mm, as recommended by NTC 2018 (NTC 2018).

The compressive strength is computed from the value proposed by the Italian code (NTC, 2018), using the ratio between the Young's modulus obtained from the test (1050 MPa) and the minimum from the code (1200 MPa). Then, the value of tensile strength $f_t$ is equal to 1.5 times the shear strength $\tau_0$ (Vinci 2012), which is also obtained from the Italian code (NTC, 2018):

$$f_t = 1.5\tau_0 \,. \tag{4}$$

For the Mode I fracture energy, given the macro modeling approach and the scarce information about the brick, mortar, and their interface, an average value of 0.012 N/mm can be assumed, as recommended by (Angelillo et al. 2014), in the absence of more information. The estimation of the compressive fracture energy is based on the ductility index in compression, defined as the ratio between the fracture energy and compressive strength (Lourenco 2009). The ductility index in compression is set equal to:

$$\boldsymbol{d_c} = 2.8 - 0.1fc \tag{5}$$

where $d_c$ is the ductility index in compression in mm and $f_c$ is the compressive strength in MPa. Consequently, the compressive fracture energy is given by:

$$Gc = d_c \cdot fc \tag{6}$$

where $G_c$ is the compressive fracture energy and $f_c$ is the compressive strength in MPa.

### *FE Model description*

Modeling the material behavior and the complex geometry needs advanced computational tools based on a nonlinear Finite Element (FE) approach, which is crucial to characterize the performance of historical structures. In the present work, DIANA 10.3 and Midas FX+ 3.3.0 (TNO 2019) are the software used to prepare the model, run the analysis and post-process the results. The FE model of the double dome and south eyvan developed by Dinani (2019) has been modified in this work to include the I-beam net of eyvan strengthening and the contribution of the adjacent structures, resulting in the updated version of Destro Bisol (2019). The final FE model prepared for the present study is shown in Figure 8. Beyond excluding the wooden components due to the joints weakness, the two minarets are not a part of the global FE model for several reasons: (a) the focus of the present study is the hybrid double dome (HDD); (b) the early-expected failure of the minarets becomes a non-problem; (c) the large increase in complexity and number of elements in the mesh modeling is avoided. The role of the wooden elements in the structural system and construction process of the Shah Mosque's HDD was discussed in (Dinani et al. 2019). The steel profile properties of the net strengthening of eyvan and encircling ties of the outer dome are made of steel profiles IPN 140, according to onsite measurements.

The updated model has 294 782 nodes and 1 412 622 elements, including four-node tetrahedron solid of type TE12L elements to represent the masonry, linear two-node embedded beam reinforcement of type L12BEA elements to characterize the strengthening encircling steel ties for the dome, and two-node spring elements of type SP2TR to model the reinforcing I-beams tying the base of the dome. The discretization process allows transforming the geometrical representational into stress analysis, in which the mesh quality, shape, and size of the elements are directly linked with the solution accuracy (TNO 2019; Wawrzynek et al. 1994).

Therefore, attention should be paid to the discretization of the mesh, giving a fair compromise between accuracy and computational efforts, to obtain a reasonable solution, in particular when non-linear, static or dynamic, analysis is performed. With this aim, in the meshing procedure of this particular building (in terms of size and shape) three approaches are used: (a) the mesh size is assigned as a function of the size of the specific element of the building; (b) the mesh has been refined around discontinuous zones (edges and faces); and (c) linear analysis is used to evaluate the presence stress or strain concentrations. Refining the mesh in areas where stresses concentrate and are prone to cracking can help to better represent the behavior of these parts, especially during subsequent non-linear analysis. The methodology described is adopted in order to reduce the number of elements but at the same time to obtain a finer mesh in the structural elements with small dimensions. In the end, the element size varies from 0.7 m in the body of the building to 0.2 meter in the upper part of the domes.

As a quasi-brittle material, masonry has a nonlinear and post-peak softening behavior. The accurate simulation, through FE models, of this behavior requires the conversion from the elastic stage to an inelastic behavior that involves cracking, leading eventually to failure (Lourenco 1996; 2002). It is important to notice that the non-linear properties involved only the FE model, and not the boundary conditions that represent the adjoining structure, modelled as linear springs in order to reduce the computational burden. This simplification is justified by the fact that the structural response is mainly governed by the dome and the eyvan, areas where the material non-linearity is expected to concentrate. Further, the adjacent volumes are two self-supporting structures with eight vaults seated on the specific stone columns independent from the investigated structure (Fig. 1(c)), 2(a)). The use of linear springs to model the adjacent structure is considered an acceptable approximation. Figure 8 shows how the boundary conditions have been applied in the FE model. For the nonlinear analysis, the total strain crack model (TSCM) has been adopted in DIANA with a rotating crack formulation. In this model, the stress-strain relationship is evaluated in the main directions of the strain vector, which simultaneously define the direction of the crack opening (TNO 2019). The input data for the TSCM comprises firstly, the basic properties of linear elasticity such as density, Young's modulus and Poisson's ratio, and secondly, the definition of the behavior in compression and tension related nonlinear material characteristics. Here, the tensile behavior is identified by an exponential softening curve and the compressive behavior by a parabolic curve followed by an exponential curve, based on the definition of the tensile and compression fracture energy (Fig. 5) (Lourenco 1996). Table 2, introduced in the previous section, gives the mechanical properties of the material.

The nonlinear analysis needs an incremental-iterative procedure to reach equilibrium at the end of each increment by using an iterative solution algorithm (TNO 2019). Furthermore, convergence problems afflict incremental analyses, which especially for complex structures, can severely affect the analysis time and the results. In the FE nonlinear analysis of complex structures, such as the Shah mosque, the search for convergence is one of the biggest challenges. To overcome the problem, several strategies were applied in the present work. Force control is utilized for the load incremental procedure, which required the use of the arc-length method to obtain the post-peak behavior. Regarding the iterative solution algorithm for incremental analysis, the secant method and the Newton Rapson modified are exploited to get the peak and post-peak responses, respectively, and the energy norm has been chosen for the convergence criteria, with a tolerance of $10^{-3}$.

### *Dynamic identification tests and boundary condition evaluation*

Dynamic identification tests have been carried out to characterize the modal parameters of the Shah Mosque, namely the natural frequencies and the modes shapes. This type of test provides a better understanding of the global behavior of heritage structures as a non-destructive evaluation and is a fundamental tool to calibrate the numerical model. The so-called Operational Modal Analysis (OMA) using environmental vibrations as a source of excitation was used, together with ARTeMIS to extract experimental modal's parameters ARTeMIS Modal. (2015).

The ambient vibration testing performed on the Shah Mosque took place in June 2019. The dynamic tests were performed using uniaxial accelerometers placed in 14 different points on the inside and outside of the double dome within seven test setups (Fig. 4(b),(c),(d)). Approximately 20 minutes reading was acquired in each setup using a sample frequency rate of 200 samples/s with ambient vibration. The modal response of a preliminary numerical model determined the accelerometer locations, intended to identify the main translational movements of the structure in the horizontal directions (X and Y). The piezoelectric accelerometers (PBC model 393B12) used in each setup have a measurement range of 0.5 g pk, sensitivity of (±10%) 10,000 mV/g, and a frequency range of (±5%) 0.15 to 1000 Hz. The accelerometers are mounted to a wooden base, which is glued to the structure to allow easy removal (PCB 2002).

The results are analyzed with ARTeMIS, processing all test setups simultaneously using two modal identification methods: Enhanced Frequency Domain Decomposition (EFDD) and Stochastic Subspace Identification based on Unweighted Principal Component (SSI-UPC), as the most widely used frequency and time domain algorithms (Brincker et al. 2000). Fig. 6 provides the value of the first frequency based on EFDD and SSI methods. The mode shapes obtained by the two methods can be compared by means of the Modal Assurance Criterion (MAC) (Ewins 2000), as one of the most popular tools for the quantitative comparison of modal vectors. The MAC takes a value between 0 and 1 representing a degree of consistency between mode shapes (Pastor 2012). The MAC is given by:

$$MAC(A,X) = \frac{\left|\sum_{j=1}^{n}\{\varphi_A\}_j\{\varphi_X\}_j\right|}{\left(\sum_{j=1}^{n}\{\varphi_A\}_j^2\right)\left(\sum_{j=1}^{n}\{\varphi_X\}_j^2\right)} \tag{7}$$

as the normalized scalar product of any two sets of vectors $\{\varphi_A\}$ and $\{\varphi_X\}$.

A model of the Shah Mosque with simplified geometry and fixed-base is generated in the ARTeMIS, where the accelerometers are applied in the position and direction to replicate the in situ configuration. The first vibration mode identified has a frequency of 2.55 Hz, and the second mode found has a frequency of 3.02 Hz, which are the translational mode in the Y (along the eyvan direction) and X direction (transversal to the eyvan direction), respectively (Fig. 7). The 2$^{nd}$ mode excites mainly the dome of the Mosque, meaning that it is not sufficient to calibrate the normal stiffness of the adjacent structure on both sides of the main body supporting the dome. Nevertheless, the information gathered from the two vibrating modes can assist in further validation of the numerical model.

Following the identification of the structure's dynamic properties, the correlation between the experimental and the numerical modal responses was examined (Fig. 7). The numerical model is updated to closely simulate the observed behavior of the structure and the stiffness of the remaining parts of the mosque adjacent to the studied volume (Fig. 8) is considered in the model as boundary conditions. Assuming the obtained elastic properties of the material through the sonic tests, acting on the boundary condition allows for modification of the dynamic properties of the numerical model. The boundary conditions are introduced as interface elements of type T18IF whose stiffness is estimated by computing the axial rigidity of the adjacent structure. According to Timoshenko's theory, the stiffness of the element considers both flexural and shear deformation as a first approximation, assuming it is free to translate at the end.

The model calibration was an iterative process that consisted of running a series of eigenvalue analysis in DIANA and comparing the results with the experimental ones in terms of frequencies and mode shapes. Excluding the geometry of the structure, the parameters that influence the linear dynamic response of the structure are mainly the boundary conditions and the properties of the material. Considering the latter as known data, as obtained through sonic tests (and accepting the level of error resulting from this estimation), the only parameter modified in each iteration was the stiffness of the springs modeled at the connection with the adjacent structure. It is noted that the evaluation between the numerical model and the experimental results is performed by the values obtained from the time-domain parametric methods of the SSI rather than the non-parametric methods of EFDD, mainly influenced by ambient responses (Ramos et al. 2011). The shear stiffness is initially estimated as 40% of the normal stiffness (similarly to continuum mechanics), and is subsequently modified to minimize the difference between the experimental and numerical models. In the end, the lateral stiffness used is 50% of the normal one to reach a similar behavior between experimental and numerical results (Fig. 7). The results, in terms of frequency and shape of the modes, are consistent with the experimental data, with an average error in the frequencies of 7%. The MAC values obtained comparing the numerical with the experimental response for the first and second modes are 0.86 and 0.81 respectively, which indicate good consistency of the modes (Table 3). Additionally, Table 4 shows the results of the numerical eigenvalue analysis performed, including information of the first ten modes of the structure. The results highlight the two first modes as the predominant ones, showing a significantly higher mass participation.

## STRUCTURAL BEHAVIOR UNDER VERTICAL LOADING

### *Behavior with stiffening walls*

After the calibration process, the model is considered reliable to simulate the structural behavior of the dome. Aiming to better understand the structural behavior of the mosque under vertical loading, several analyses were carried out under self-weight considering different scenarios. These analyses were meant to: (1) study the influence of the stiffening walls connecting the domes; (2) study the influence of the material post-peak behavior, measured by the fracture energy in tension and compression; (3) study the influence of the soil on the structural response; and (4) study the role of the strengthening of early 20$^{th}$ century. These scenarios were evaluated by means of nonlinear incremental vertical analysis, allowing to better understand the structural performance of the Shah Mosque and to evaluate the structural safety under vertical loading.

The first analysis was carried out in a model fixed at the base, as usual in most structural analysis. The building is subjected to gravitational loading until failure. The capacity curve for the vertical loading analysis indicates the vertical displacement at the top of the dome, as a control point, versus the vertical load factor (Fig. 9(a)). It is noted that a load factor of one represents the application of 100% of the self-weight of the structure. As the graph demonstrates, the capacity curve has a linear behavior up to the load factor of about 2, where a change of stiffness indicates damage in the structure. The structure can tolerate the vertical load up to 2.35 times the self-weight in the peak point. The largest displacements occur at the top of the dome (Fig. 9(b)). Besides, the concentration of the principal tensile strain E1, in the dome and the semi-dome of the eyvan, leads to the formation of several cracks (Fig. 9(c). The resulting damage of eyvan represents the restrained deformation of a crack in the west side of the semi-dome that the historical document of Salnameh reported in 1935 (Fig. 3(a)). The large values highlight the tendency of the bulbous dome to detach from the wall opposite to the eyvan and large closed arch (Fig. 9(d)), illustrated by the presence of the large compressive strains (induced by the combination of large compressive and shear stresses) at the point where the double dome rests on (Fig. 9(d),(e)). The incremental displacement (Fig. 9(f)) for this load factor 2.35 presents how the failure mechanism prior to the peak is governed from the inflection of the thin outer shell of the dome, mainly in the upper portion where the dome intends to detach from the stiffening walls. At the end of the capacity curve, the tensile and compressive principal strains (Fig. 9(g),(h)) and incremental displacement (Fig. 9(i)) underline how the final failure mechanism is determined from the high shear stress in the drum on the southern wall.

### *Sensitivity analysis for fracture energy*

A key point related to the reliability of numerical analysis is to know the importance of the material parameters and their influence on the structural response (Lourenco 1998). Given the difficulties in the precise determination of the fracture energy values for masonry, understanding the impact of this property in the collapse mechanism and in the ultimate load factor is critical. For that matter, a sensitivity analysis was carried out varying the values initially assumed for the fracture energy: 1) ideal-plastic behavior in both compression and tension, meaning infinite fracture energies; 2) ideal plastic behavior in tension with estimated fracture energy in compression; 3) ideal plastic behavior in compression with estimated fracture energy in tension. Fig. 10(a) displays the capacity curves of the results in comparison with the case where predicted values for material properties are used, which highlights the relevance of the fracture energy in terms of ultimate capacity and ductility.

The capacity curve for the model including infinite fracture energy in both compression and tension reveals how these factors influence not merely the strain capacity but also the ultimate loadbearing capacity, with an increase of 50% in load capacity. Plotting the principal tensile and compressive strains for a load step near failure helps to understand the collapse mechanism of the structure (Fig. 10(b)). The compressive strains at the base of the eyvan's inner arch and the shear on top of the closed southern arch (opposite to eyvan), prove the tendency of the double dome to push down the underlying elements. Furthermore, the fracture energy can influence not only the capacity of the structure in terms of ultimate load and deformation but also the collapse mechanism. In this case, damage concentrates in the stiffer lower portions of the building, and no collapse appears in the outer dome.

In case ideal plastic behavior is only considered in tension or compression, the analysis offers not only capturing the influence of the fracture energy but also which mechanism is determinant in the response of the structure. The examination of the capacity curves (Fig. 10(a)) illustrates how the tensile fracture energy controls the response of the structure prior to the peak and the fracture energy in compression impacts the post-peak behavior, with moderate influence in the value of the ultimate load and displacement at peak. The collapse mechanisms vary significantly in the two cases, meaning that two different mechanisms are competing. In the case of predicted fracture energy in tension and infinite in compression, the principal tensile strain in a load stage close to the collapse (Fig. 10(c)) highlights the loss of bearing capacity that happens due to the tendency of the dome to detach from the stiffening walls. This behavior is similarly recognizable when the predicted fracture energy is used in both tension and compression, for a load stage close to the peak (Fig. 9(g)(h)(i)). In the case of predicted fracture energy in compression and infinite in tension, the analysis of the principal strains (Fig. 10(d)) shows how the collapse is due to both the high shear stress in the lower part of drum on the closed Southern arch and the large compression deformation on the supports of the eyvan's inner arch. These results, in comparison with the case of predicted fracture energy, prove the compatibility with the behavior of the structure in post-peak phase, although the higher fracture energy in compression provides greater shear strength. This involves the loading of the eyvan's inner arch, which contributes to the resistant mechanism increasing the ultimate resistance. Beyond the emphasis on the importance of determining reliable values for the fracture energy, all the results highlight how this kind of sensitivity analysis can lead to a better understanding of the failure modes and which kind of strains/stresses are determinant. It is noted that, for an incremental iterative analysis, assuming higher values of fracture energy helps in the achievement of convergence. It is demonstrated that this should be carefully used as the collapse mechanism may be changed.

### *Behavior without stiffening walls (or stiffeners)*

The stiffeners play an indispensable role in the structural stability of the double dome, as the bulbous form is unable to contain the thrust line within the masonry to achieve an equilibrium configuration in the absence of tensile strength (Dinani 2019). In this regard, the global masonry structure, with no stiffeners, is subjected to the incremental vertical analysis to explore the importance of these elements.

The capacity curve indicates how the double dome cannot resist self-weight (Fig. 11(a)). The ultimate load is around 3 times less than the model with the stiffeners, besides, the deformation capability indicates an important reduction. The incremental displacements confirm that the collapse is due to a ring hinging of the outermost area of the external dome (Fig. 11(b)). The maximum principal tensile strains (Fig. 11(c)) show the formation of several radial cracks in this part of the dome and also the ring cracks. For a load factor of about 0.5, cracking of the outer dome becomes relevant with major radial cracks in the outer dome, Fig. 11(c). This analysis along with documented vertical cracks (Fig. 3(c)) in the intersection of the stiffening walls and the outer dome emphasizes the major contribution of the stiffeners and their connection in compensating the weakness of the bulbous shape made of a material with low tensile strength. These considerations lead to an important reflection on the safety level of the mosque and the loadbearing capacity of the dome, which is intensely dependent on the stiffening walls and their connections to the external dome and may require strengthening intervention, in case of cracks or inadequate interlock. This discussion also demonstrated that the traditional encircling wooden ties system, the strengthening of 1940s using encircling steel ties and the wooden elements that may provide some connection between stiffening walls and dome, are essential for the equilibrium state of the entire double dome. Note that the wooden elements are claimed to have mostly contributed in the intermediate configuration of the construction sequence to make a hybrid structure (Dinani 2019).

### *The soil effect and the structural response*

Soil settlements can help to determine the actual cause of existing damage (Roca et al. 2010), as they cause displacements, damage and cracks in the building. Therefore, the interaction of the structure with the soil is taken into account by performing a sensitivity analysis varying the soil stiffness through an incremental vertical analysis for the global model. Using the Standard Penetration Test (SPT) carried out for the construction of the Esfahan metro, the soil properties were obtained. The elastic modulus found using (Denver 1982) provided the basis on which the interface normal stiffness is equal to 13 MN/m$^3$. It should be noted that Moarefi (Salnameh-e Maaret-e Esfahan, Sal-e Tahsili 1313-1314 1935) strengthened the foundation of the mosque in some parts in 1932. He pointed out that the acceleration of building process, due to large number and time limitation of Safavid projects, could be the main reason of the structural weakness of the foundation (Varjavand 1976).

The capacity curves demonstrate that the response of the structure in terms of global stiffness and ultimate strength is much dependent on the soil deformability, with a reduction of capacity of about 50% due to the consideration of the soil stiffness (Fig. 12(a)). The analysis with the above calculated soil stiffness for a load stage close to the peak displays the collapse mechanism mainly due to the overturning of the southern wall containing the closed arch (Fig. 12(b)). The crack distribution on the double dome, which can be inferred from the principal tensile strains, confirms that failure mechanism (Fig. 12(c)). The tensile strains accumulate in the connection between the southern wall and the rest of the structure. This behavior due to differential settlements in the structure could have been realistic if the structure had been built in one moment, a unreasonable assumption for historical structures. Then the modeling of the soil should consider the building process through a phased analysis by applying the load following the construction process. Given the self-weight of the two minarets and the strengthening of the foundation in parts of the mosque by Moarefi (Salnameh-e Maaret-e Esfahan, Sal-e Tahsili 1313-1314 1935), by doubling and tripling the soil stiffness, which show some approximation of the original stiffness of the rigid-foundation analysis but a lower gain of the original maximum capacity.

### *Behavior of structure with the strengthening of the early 20$^{th}$ century*

In 1932, the mosque was in danger of the collapse and structural strengthening was applied. To explore the effect of the strengthening system on the structural response due to the vertical loading, the FE model contains a net of tie beams applied on the eyvan and encircling ties system of the outer dome. The capacity curve for an incremental vertical analysis (Fig. 13(a)) indicates an increase in terms of ductility. The analysis in terms of principal tensile strain at the end of the capacity curve, (Fig. 13(b)), shows that the failure mode mainly happens due to the tendency of the dome to push on the underlying structure, which causes shear in the top of the Southern wall and the eyvan's inner arch. This behavior triggers important compression and tensile strains (Fig. 13(b),(c)) in the entire contact surface between the double dome and the underlying part of the building. These observations, if compared with the results obtained from the model without strengthening, are valuable information. By reducing the flexibility of the dome, the tie rod strengthening provides higher tensile strength and impacts the behavior before the peak. It contributes to the absorption of the outer dome’s horizontal thrust in the case of weakness in joints between the dome and the stiffening walls or the absence of wooden elements. Besides, the net strengthening of the eyvan has removed the large crack of the semi-dome (Fig. 9(d), Fig. 13(b)). In situ observation also proves the restraint crack of semi-dome by I-beams strengthening of 1932. The steel reinforcement elements of the semi-dome impact the ductility and in consequence the post-peak behavior.

## SEISMIC ANALYSIS

### *Pushover analysis for unreinforced structure*

A pushover analysis is performed to study the seismic behavior of the Shah Mosque with the reinforcement system, which represents the actual condition, and without the reinforcement system to discuss its contribution. Typically, historical masonry structures were designed for vertical static loads rather than high inertial lateral loads that earthquakes cause. Moreover, the in-plane strength of the masonry elements is significantly higher than its out-of-plane stiffness (Lourenco et al. 2011). Thus, the present analysis investigates the structural performance and explores the contribution of the strengthening system in the seismic and collapse mechanisms.

The accuracy of the pushover analysis is strongly related to the regularity of the structure (CEN 1998-1 2004). In the case of complex structures, such as the mosque, the measure of this regularity can be evaluated through modal analysis. In the case at hand, modal analysis shows how the structure is mainly characterized by two translational modes and higher modes have small percentage of participation masses (Table 4). This behavior reduces possible torsional effect during seismic action and increases the reliability of the pushover analysis. The two translational main modes of the structure and the use of a load profile proportional to the masses make the pushover analysis an effective tool to understand the seismic response of the structure, allowing to determine the ability of a structure to resist horizontal loading in the two directions identified by modal analysis.

With this aim a pushover analysis with a horizontal load pattern proportional to the mass of the structure is assumed, which corresponds to the first distribution of lateral forces defined by Eurocode 8 (CEN 1998-1 2004). The method uses an incremental-iterative procedure assuming conditions of constant gravity loads and monotonically increasing the horizontal loads. This method can be used to estimate the failure mechanisms of the structure, to analyze the distribution of damage, to assess the structural performance and to predict the capacity curve (CEN 1998-1 2004). For this analysis, the same approach and settings employed for the previous incremental vertical examination are used. The results will be expressed in terms of base shear factor $\alpha$ (g) versus a control point displacement $\delta$ (m). The factor $\alpha$ is given by:

$$\alpha = \frac{\sum F_H}{\sum F_V}\ [g] \tag{8}$$

where $\sum F_H$ is the sum of the horizontal forces applied to the structure and $\sum F_v$ is the sum of the vertical reactions.

In the following, horizontal loading is taken into account in both longitudinal (±Y) directions and, due to the almost symmetrical configuration of the structure, only in the transversal directions of (-X). Regarding the selection of the control point, it is noted that this was chosen according to the observed collapse mechanism. All curves are thus plotted for the control points that show the maximum displacement for each analysis. In this case, the top of the eyvan is chosen for the +Y direction and the top of the external dome for the -Y and -X directions.

The capacity curve obtained from the pushover analysis for the unreinforced model can be found in Fig. 14. Note that the initial horizontal movements due to the vertical loading are small and have been removed from the plots in order to focus on the response due to lateral loading. In the +Y direction, despite the fact that the maximum shear factor of 0.20 is lower than the value of 0.22 in the -Y, the capacity in terms of ultimate displacement and ductility is increased. It is possible to find the reason for this different behavior in the two clearly different collapse mechanisms observed in each direction, one of them involving the dome and the other the eyvan. The incremental displacement exhibits the out of plane failure mechanisms of the eyvan in the +Y direction, The principal tensile strains show clearly the failure mechanism consisting of the detaching of the arch frame of the eyvan from the semi-dome (Fig. 16(a),(b)). Besides, the performance of the double dome in the collapse mechanism is remarkable. The observation emphasizes that there is a small bump in the capacity curve before the peak point. This behavior mainly refers to the strength loss of the connection between the stiffening walls and the inner dome.

Regarding the pushover in -Y direction, at the post-peak stage, the outer dome presents the largest displacements in the outer dome, where the failure mechanism takes place (Fig. 16(c)). The analysis of principal tensile strains (Fig. 16(d)) points out how the outer dome drag the stiffener walls to detach from the inner dome.

Concerning the -X direction, the structure can resist a base shear factor of 0.24, which is the highest among all longitudinal directions. The incremental displacement in the -X direction and the principal tensile strains (Fig. 16(e),(f)) reveal a similarity in the performance of the double dome and collapse mechanism to the pushover in -Y direction, consisting of the detachment of the stiffener walls from the domes. This behavior tends similarly to trigger large cracks in the outer dome. Although the structural performance in the -X and -Y are alike, the resistance to horizontal forces are dissimilar due to the different arrangement of the radial walls and the stiffness provided by the adjacent structure. The response in the X direction appears more fragile and has the greatest maximum capacity. The resulting damages from numerical pushover analysis seem to reproduce the existing damage pattern in the semi-dome of eyvan (Fig. 15(a)). Thus, the pushover analysis reveals the double dome and the eyvan as the most vulnerable parts of the structure in case of an earthquake, which demonstrate the need and correctness of the reinforcement system of the 1930s.

### *Pushover analysis for structure with the strengthening of early 20$^{th}$ century*

The model that includes the strengthening of the Shah Mosque, comprising a net of I-beam and encircling ties system, is subjected also to the pushover analysis to assess the effectiveness of the reinforcement and its efficiency to improve the seismic performance of the mosque. The results derived from the capacity curve indicate an increase in terms of ultimate loadbearing capacity and ductility for the reinforced structure (Fig. 14). In the +Y direction, the reinforced structure raises the ultimate capacity of the Shah Mosque about 25%. The incremental displacements in the post-peak phase exhibit the out of plane mechanism of the façade (Fig. 16(g)), which is quite similar to the unreinforced model. The comparison in terms of principal tensile strains (Fig. 16(b) and Fig. 16(h)) highlights the contribution of the reinforcements elements. Firstly, the encircling ties system provides a confinement effect by reducing the deformation of the outer dome, with a tendency of the stiffening walls to detach from the domes. The tops of the stiffeners control the failure mechanism. Secondly, the networks of beams in the eyvan provide increased strength in the out-of-plane mechanism and a reduction of deflection.

The analysis in the -Y direction confirms an increment of the loadbearing capacity of around 30% for the reinforced model (Fig. 14). For a load stage in the post-peak phase, the failure mode can be identified. As previously mentioned the tie-beam system of the dome gives a strong confinement effect for the +Y direction. This confinement also changes the structural response along -Y, which appears more global (Fig. 16(i),(j)). The damage is no longer concentrated only in the double dome, but also other portions of the building are involved in the load resistant mechanism. The global response tends to trigger a collapse mechanism consisting of the dome overturning together with its underlying structure, in the applied forces direction (Fig. 16(i)).

Concerning the behavior of the reinforced structure in the -X direction, the capacity curve (Fig. 14) shows an increase of ultimate strength and ductility that draws an analogy with the response in the -Y direction. Hence, the incremental displacements in the post-peak phase show a large movement of the outer dome leading the structure to failure (Fig. 16(k)). The analysis of the principal tensile strains shows the detachment of the stiffening walls from the inner dome (Fig. 16(l)).

The comparison with the unreinforced model (Fig. 16(e),(f)) highlights the confinement effect of the tie rods, which lead to a more global structural response in the -Y direction. The capacity curves show that the softening branch is particularly similar for the two cases, thus confirming the collapse mechanism, or rather the large displacement in the outer dome and the detachment of the stiffening walls from the inner dome. Furthermore, the greater capacity in the -X direction confirms, in the case of the structure without reinforcement indicates that the adjacent structure may provide an important contribution to the response.

## CONCLUSION

The current paper studies the structural performance of the Shah Mosque, due to the vertical and horizontal actions through nonlinear analysis.

An experimental in-situ investigation using NDT, including sonic tests and dynamic identification tests, was carried out in different parts of the studied volume. The sonic tests evaluate the elastic properties of the material, while the dynamic identification test reveals the properties of a structure in terms of natural frequencies and vibration modes. The results of the dynamic identification tests were used for the calibration of the FE model and the boundary conditions. The updated FE model includes the structural intervention of the 1930s, and the contribution of the adjacent structures, trying to carefully simulate the real condition of the structure.

The incremental nonlinear analysis indicates that the structural response under gravitational loads has an adequate safety level. However, the double dome is not able to withstand its self-weight without the stiffening walls. The indisputable structural role of the stiffening walls to prevent the horizontal thrust of the bulbous dome is demonstrated and the importance of the connection between these and the domes is stressed. This also justified that past strengthening including a metal encircling ring for the outer dome. Also, the role of the eliminated wooden components from the model due to the joint weakness should be considered in the construction process, improving the connections of the masonry elements and equilibrium state of the Shah Mosque's masonry bulbous dome.

The examination of the influence of mechanical properties, such as fracture energy, nurtures Shah Mosque's structural studies to fully understand the structural behavior and the collapse mechanism when the structure is subjected to its weight. Through this study, two competing failure mechanisms (one more related to the double dome and another more related to the supporting body of the dome) and the two weaker parts of the structure are identified. The influence of the fracture energy on the collapse mechanism is thus observed. Additionally, sensitivity analysis for the soil stiffness through an incremental vertical analysis investigates the influence of the soil on the structure. The results for the soil stiffness provide the collapse mechanism as an overturning of the southern massive wall, the only one without opening, which justifies some of the past strengthening of the foundations.

The pushover analysis for the unreinforced model demonstrates the vulnerability of the double dome and the eyvan. The longitudinal orientation of the Mosque is the most vulnerable, especially for loadings acting in the positive direction, +Y, for which a maximum base shear factor of 0.20 is obtained. The collapse mechanism obtained consists of the overturning of the façade of the eyvan. Yet, the horizontal response in the transversal direction, +X, shows the greatest maximum capacity but the collapse occurs in a fragile way. Taking the strengthening system into consideration increases the ultimate capacity of the Shah Mosque almost 30% and also influences the ductility. The encircling ties system of the outer dome improves the integrity of the structural elements, in particular, the stiffening walls and the domes. The network of I-beams strengthening provides an increased strength in the out-of-plane mechanism of the eyvan and reduces the deflection of the semi-dome. The outcomes show the efficiency of the structural intervention of the Shah Mosque, which leads to a more global structural behavior.

The semi-dome of the eyvan presents a restrained deformation crack during the inspection, which was reported in the historical document of Salnameh in 1935. The weakness of the connection between the stiffening walls and bulbous dome, has caused the existing damages of both the outer dome and semi-dome, approved by the cracks pattern and numerical analysis. This further demonstrates the integration between historical evidence, inspection and FE analysis.

The lateral loading in the +Y, as the most vulnerable direction, appears to be decisive for seismic assessment, which as only a moderate capacity. Therefore, a structural health monitoring system would be beneficial to further analyze the present condition and to further contribute in identifying and evaluating existing damage and assessing the structural safety.

## DATA AVAILABILITY STATEMENT

Some or all data, models, or code that support the findings of this study are available from the corresponding author upon reasonable request.


## ACKNOWLEDGEMENT

Special thanks to the Esfahan Cultural Heritage Organization, the staff of Meidan Naghsh-e Jahan World Heritage Site, and restoration workshop of the Shah Mosque to facilitate in situ experimental tests that supported by the SAHC MSc programme in Structural Analysis of Monuments and Historical Constructions.


## NOTATION

The following symbols are used in this paper:

$\alpha$ (g) = base shear factor;

$a_g$ = peak ground acceleration, PGA;

$d_c$ = ductility index in compression (mm);

E = Young's modulus of masonry (MPa);

$F_0$ = maximum spectral amplification;

$f_c$ = compressive strength (MPa);

$f_t$ = tensile strength;

$G_c$ = compressive fracture energy (N/mm);

$\tau_0$ = tensile strength;

$\{\varphi_A\}$ = modal vector;

$\{\varphi_X\}$ = modal vector;

MAC = Modal Assurance Criterion;

ρ = mass density of masonry ($Kg/m^3$);

$S_e$ = seismic demand;

$V_P$ = P-waves velocity;

$V_R$ = R-wave velocity;

ν = poisson's ratio;

$\Sigma^{FH}$ = sum of the horizontal forces

$\Sigma^{Fv}$ = sum of the vertical reactions

# REFERENCES


*Akhgar Newspaper*. 1936. "Akhgar Newspaper No. 1161." Esfahan.

*Akhgar Newspaper*. 1941. "Akhgar Newspaper No. 1891." Esfahan.

Angelillo, M., P. B. Lourenço, and G. Milani. 2014. "Masonry behavior and modelling." In Vol. 551 of *Mechanics of masonry structures, CISM international centre for mechanical sciences*, edited by M. Angelillo. Vienna: Springer. https://doi.org/10.1007/978-3-7091-1774-3_1

ARTeMIS Modal. 2015. *SVS-structural vibration solutions A/S*. Aalborg, Denmark: Structural Vibrations Solutions A/S.

ASTM. 2009. *Standard test method for pulse velocity through concrete*. West Conshohocken, PA: ASTM.

Berra, M., L. Binda, L. Anti, and A. Fatticcioni. 1992. "Utilisation of sonic tests to evaluate damaged and repaired masonries." In *Proc., Conf. On Nondestructive Evaluation of Civil Structures and Materials*, 329–338. Boulder, CO: Atkinson-Noland and Associates.

Binda, L., A. Saisi, and C. Tiraboschi. 2000. "Investigation procedures for the diagnosis of historic masonries." *Constr. Build. Mater*. 14 (4): 199–233. https://doi.org/10.1016/S0950-0618(00)00018-0

Binda, L., A. Saisi, and C. Tiraboschi. 2001. "Application of sonic tests to the diagnosis of damaged and repaired structures." *NDT & E Int.* 34 (2): 123–138. https://doi.org/10.1016/S0963-8695(00)00037-2

Binda, L., L. Cantini, A. Saisi, and C. Tiraboschi. 2007. "Use of flat-jack and sonic tests for the qualification of historic masonry." In *Proc., 10th North American Masonry Conf. 10NAMC*, 791–803. Longmont, CO: Masonry Society and Related Masonry Industry Organization. http://hdl.handle.net/11311/248260

Binda, L., and A. Saisi. 2009. "Application of NDTs to the diagnosis of historic structures." In Proc., *NDTCE 2009, Non-Destructive Testing in Civil Engineering—NDTCE'09*, 43–69. Paris: Central Laboratory of Bridges and Roads.

Brincker, R., L. Zhang, and P. Andersen. 2000. "Modal identification from ambient responses using frequency domain decomposition." In *Proc. 18th Int. Modal Analysis Conf. (IMAC).* San Antonio: Society for Experimental Mechanics.

CEN (European Committee for Normalization). 2004a. *Eurocode 8: Design of structures for earthquake resistance—Part 1: General rules, seismic actions and rules for buildings*. EN 1998-1. Brussels, Belgium: CEN.

CEN (European Committee for Normalization). 2004b. *Testing concrete Part 4: Determination of ultrasonic pulse velocity*. EN 12504-04. Brussels, Belgium: CEN.

Circular n° 7 of NTC 2018. 2019. *Istruzioni per l'applicazione dell'«Aggiornamento delle Norme tecniche per le costruzioni*. Referred to in the ministerial decree 17 January 2018: Rome: Ministry of Sustainable Infrastructure and Mobility.

Croci, G. 1998. Vol. 1 of *The conservation and structural restoration of architectural heritage*. Southampton, England: WIT Press.

Denver, H. 1982. "Modulus of elasticity for sand determined by SPT and CPT." In *Proc., 2nd European Symp. on Penetration Testing (ESOPT-2)*. London: Routledge.

Destro Bisol, G. 2019. "Safety assessment of the Shah Mosque in Isfahan, Iran." M.Sc. thesis, Dept. of Civil Engineering, Universidade do Minho.

Dinani, A. T. 2019. “Hybrid double dome: Building performance and cable-net strengthening of Esfahan Shah Mosque’s dome.” Ph.D. thesis, Politecnico di Milano. http://hdl.handle.net/10589/145709

Dinani A.T., Sadeghi S., Lourenço P.B. (2019) A Double Dome Through the Ages. In: *Aguilar R., Torrealva D., Moreira S., Pando M.A., Ramos L.F. (eds) Structural Analysis of Historical Constructions*, 87-95. RILEM Bookseries, vol 18. Cham: Springer. https://doi.org/10.1007/978-3-319-99441-3_8

Everett, M. E. 2013. *Near-surface applied geophysics*. Cambridge, UK: Cambridge University Press.

Ewins, D. 2000. *Modal testing: Theory, practice and application*. 2nd ed. Hertfordshire, UK: Research Studies Press.

Heyman, J. 1995. *The stone skeleton: Structural engineering of masonry structures*. Cambridge, UK: Cambridge University Press.

Hosseini Jonabadi, M. H. 2000. “Rozat Al-safaviyeh.” In *Dr. Afshar’s endowment foundation, Tehran, H. Jonabadi M H (1617) Rozat Alsafaviyeh, Esfahan*, 1st ed., edited by G. M. Tabatabai. Tehran, Iran: Afshar’s Endowment Foundation.

ICOMOS/ISCARSAH (International Council on Monuments and Sites/ International Scientific Committee on the Analysis and Restoration of Structures of Architectural Heritage) Committee. 2005. “Recommendations for the analysis, conservation and structural restoration of architectural heritage.” Accessed September 25, 2019. https://www.icomos.org.

Iranian Cultural Heritage Organization Documentation Center. 2003. *Naghsh-e-Ajab: Architectural drawings collection of historical monuments of Iran*. Tehran, Iran: Research Institute and Cultural Heritage and Tourism.

Lourenço, P. B. 1996. “Chapter 2: Modelling masonry: A material description.” In *Computational strategies for masonry structures*, 11–26. Delft, Netherlands: Delft University Press. http://resolver.tudelft.nl/uuid:4f5a2c6c-d5b7-4043-9d06-8c0b7b9f1f6f

Lourenço, P. B. 1998. “Sensitivity analysis of masonry structures.” In *Proc., 8th Canadian Masonry Symp.*, 563–574. Edmonton, AB, Canada: Canadian Masonary Research Institute.

Lourenço, P. B. 2002. “Computations on historic masonry structures.” *Prog. Struct. Mater. Eng*. 4 (3): 301–319. https://doi.org/10.1002/pse.120.

Lourenço, P. B. 2009. “Recent advances in masonry modelling: Micromodelling and homogenization.” *In Multiscale modeling in solid mechanics: Computational* *approaches*, 251–294. London: Imperial College Press. https://doi.org/10.1142/9781848163089_0006

Lourenço, P. B., M. Nuno, L. F. Ramos, and D. V. Oliveira. 2011. “Analysis of masonry structures without box behavior.” *Int. J. Archit. Heritage* https://doi.org/10.1080/15583058.2010.528824

Maccarini, H., G. Vasconcelos, H. Rodrigues, J. Ortega, and P. B. Lourenço. 2018. “Out-of-plane behavior of stone masonry walls: Experimental and numerical analysis.” *Constr. Build. Mater.* 179 (Aug): 430–452. https://doi.org/10.1016/j.conbuildmat.2018.05.216.

Miranda, L. F., J. Rio, J. M. Guedes, and A. Costa. 2012. “Sonic impact method-A new technique for characterization of stone masonry walls.” *Constr. Build. Mater*. 36 (Nov): 27–35. https://doi.org/10.1016/j.conbuildmat.2012.04.018.

Miranda, L. F., L. Cantini, J. M. Guedes, and A. Costa. 2016. “Assessment of mechanical properties of full-scale masonry panels through sonic methods. Comparison with mechanical destructive tests.” *Struct. Control Health Monit*. 23 (3): 503–516. https://doi.org/10.1002/stc.1783.

Monshi, I. B. 2003. “Tarikh-e alamaraye abbasi.” In *Amir kabir, Tehran: Iskanda Beg Monshi (1615) Tarikh-e alamaraye abbasi*, *Esfahan*, 1st ed., edited by I. Afshar. Tehran, Iran: Amirkabir.

Murano, A., J. Ortega, G. Vasconcelos, and H. Rodrigues. 2019. “Influence of traditional earthquake-resistant techniques on the out-of-plane behavior of stone masonry walls: Experimental and numerical assessment.” *Eng. Struct*. 201 (Dec): 109815. https://doi.org/10.1016/j.engstruct.2019.109815.

NTC (Norme Tecniche per le Costruzioni). 2018. *Norme tecniche per le costruzioni. Decree of the Minister of the Infrastructures and transportations*. Rome: NTC.

Pastor, M., M. Binda, and T. Harčarik. 2012. “Modal assurance criterion.” *Procedia Eng*. 48: 543–548. https://doi.org/10.1016/j.proeng.2012.09.551.

PCB (PicoCoulomB) . 2002. “installation and Operating Manual, vibration division”. http://www.pcb.com/contentstore/docs/PCB_Corporate/Vibration/products/Manuals/3741D4HB100G.pdf

Ramos, L. F., R. Aguilar, and P. B. Lourenço. 2011. “Operational modal analysis of historical constructions using commercial wireless platforms.” *Struct. Health Monit*. 10 (5): 511–521. https://doi.org/10.1177/1475921710388973.

Roca, P., M. Cervera, and G. Gariup. 2010. “Structural analysis of masonry historical constructions. Classical and advanced approaches.” *Arch. Comput. Methods Eng*. 17 (3): 299–325. https://doi.org/10.1007/s11831-010-9046-1.

Salnameh-e Maaref-e Esfahan, Sal-e Tahsili 1313–1314. 1935. *Esfahan Ministry of Education, Academic year 1934–35, Esfahan*. Esfahan, Iran: Ministry of Maaref, Publishing Office.

Sánchez-Aparicio, L. J., A. Bautista-De Castro, B. Conde, P. Carrasco, and L. F. Ramos. 2019. "Non-destructive means and methods for structural diagnosis of masonry arch bridges." *Autom. Constr*. 104 (Aug): 360–382. https://doi.org/10.1016/j.autcon.2019.04.021.

TNO DIANA (Netherlands Organisation for Applied Scientific Research Displacement Analyser Finite Element Analysis). 2019. *Diana finite element analysis user's manuals release 10.3*. Delft, Netherlands: DIANA FEA BV.

Varjavand P. 1976. "How the Masjed-e shah survived from the demolition". *Art and people magazine, No 164*. Tehran, Iran: Ministry of Culture and People.

Vinci, M. 2012. *Metodi di calcolo e tecniche di consolidamento per edifici in muratura: Analisi, esempi di calcolo, particolari costruttivi*. Palermo, Italy: Dario Flaccovio. ISBN 9788857909509.

Wawrzynek, P. A., B. J. Carter, A. R. Ingraffea, and D. O. Potyondy. 1994. "A topological approach to modeling arbitrary crack propagation in 3D." In *DIANA computational mechanics '94*, edited by G. M. A. Kusters and M. A. N. Hendriks. Dordrecht, Netherlands: Springer.https://doi.org/10.1007/978-94-011-1046-4_7.

**Table 1.** Results of the sonic testing on the Shah Mosque

| Zone | Vp (m/s) | Vr (m/s) | Vp/Vr | ν | CoV (%) | E (MPa) |
|---|---|---|---|---|---|---|
| Stiffening walls (I) | 1077 | 462 | 2.33 | 0.38 | 11.1 | 1083 |
| Stiffening walls (II) | 1110 | 420 | 2.64 | 0.25 | 13.1 | 1532 |
| Stiffening walls (III) | 950 | 559 | 1.70 | 0.38 | 14.6 | 911 |
| Inner dome | 821 | 373 | 2.20 | 0.34 | 9.0 | 780 |
| Outer dome | 994 | 424 | 2.34 | 0.40 | 16.1 | 968 |
| Eyvan | 936 | 420 | 2.23 | 0.38 | 22.8 | 980 |
| Average results | 980 | 440 | 2.21 | 0.36 | 14.4 | 1040 |

**Table 2.** Masonry material properties

| Material properties | Unit | Value |
|---|---|---|
| Mass density | $\rho$ (kg/m$^3$) | 1800 |
| Young's modulus | E (MPa) | 1050 |
| Poisson's ratio | $\nu$ | 0.35 |
| Compressive strength | $f_c$ (MPa) | 2.1 |
| Compressive fracture energy | $G_c$(N/mm) | 5.4 |
| Tensile strength | $f_t$ (MPa) | 0.08 |
| Fracture energy mode I (tension) | $G^I_f$ (N/mm) | 0.012 |

**Table 3.** MAC Comparison between experimental and numerical model

| Mode | Model | f (Hz) | MAC |
|---|---|---|---|
| Mode 1 | Numerical | 2.46 | 0.86 |
| | Experimental | 2.55 | |
| Mode 2 | Numerical | 2.75 | 0.81 |
| | Experimental | 3.02 | |

Note: The SSI is considered as the modal identification methods for the experimental model.

**Table 4.** Eigenvalue analysis for the first 10 modes

| **Modes** | | **X** | | | **Y** | | |
|---|---|---|---|---|---|---|---|
| **n** | $f$ (Hz) | Eff. Mass (t) | Eff. Mass (%) | Cumulative (%) | Eff. Mass (t) | Eff. Mass (%) | Cumulative (%) |
| **1** | 2.46 | 0.00 | 0.00 | 0.00 | 12900.00 | 62.90 | 62.90 |
| **2** | 2.75 | 6780.00 | 33.10 | 33.10 | 0.00 | 0.00 | 62.90 |
| **3** | 3.51 | 260.00 | 1.27 | 34.40 | 0.00 | 0.00 | 62.90 |
| **4** | 3.68 | 0.00 | 0.00 | 34.40 | 831.00 | 4.06 | 67.00 |
| **5** | 4.29 | 25.80 | 0.13 | 34.50 | 0.29 | 0.00 | 67.00 |
| **6** | 4.31 | 0.02 | 0.00 | 34.50 | 1430.00 | 6.96 | 73.90 |
| **7** | 4.53 | 1420.00 | 6.96 | 41.50 | 0.01 | 0.00 | 73.90 |
| **8** | 4.67 | 0.01 | 0.00 | 41.50 | 422.00 | 2.06 | 76.00 |
| **9** | 5.05 | 553.00 | 2.70 | 44.20 | 0.00 | 0.00 | 76.00 |

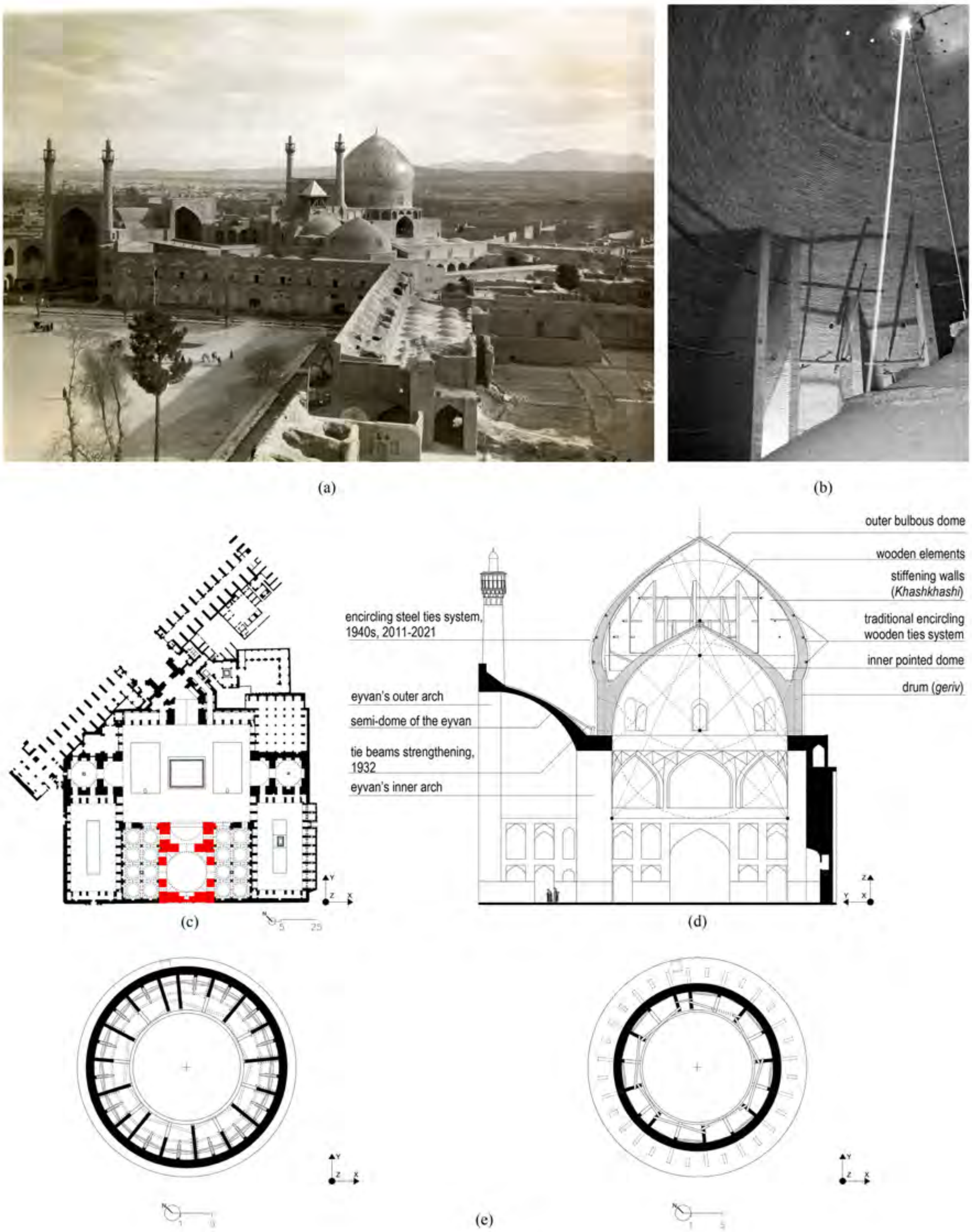


**Fig. 1.** The Esfahan Shah Mosque: (a) seen from the eyvan of Ali Qapu palace, Reprinted from ETH-Bibliothek Zürich, Bildarchiv/Stiftung Luftbild Schweiz / image by Walter Mittelholzer, 1925 / LBS_MH02-02-0160-AL-FL; (b) radial stiffening walls seen from space in-between of the domes, image by Ali T. Dinani; (c) ground floor plan and the highlighted studied volume, Modified from Iranian Cultural Heritage Organization Documentation Center 2003; (d) the hybrid double dome and eyvan in section, and (e) the arrangement of the stiffeners and wooden elements in the HDD, Reprinted from Dinani 2019, © Inter-Esse Studio.

(a)

(b)

(c)

**Fig. 2.** (a) The Esfahan Shah Mosque on the southern edge of the Naghsh-e Jahan Meidan, image courtesy of Iran Documentary / Hamid Mojtahedi / with permission; (b) encircling steel ties system of the 1940s for the bulbous dome, image by Ali T. Dinani; (c) underneath the glazed tile of bulbous dome's extrados: the encircling steel ties system (2011-2021) is placed between the existent wooden and the steel tie rods applied in 1940s. The reasoning of the recent steel tie rod application (2011-2021) seems unconvincing for the authors, image courtesy of Esfahan Naghshe Jahan UNESCO World Heritage Site Archive Center / photographer: Hossein Pakdel, 2015 / with permission.

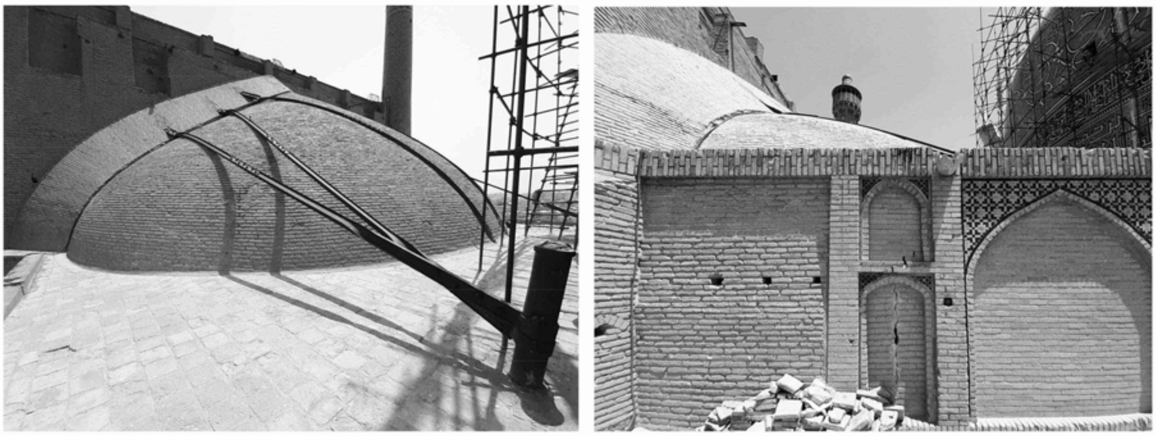

(a) (b)

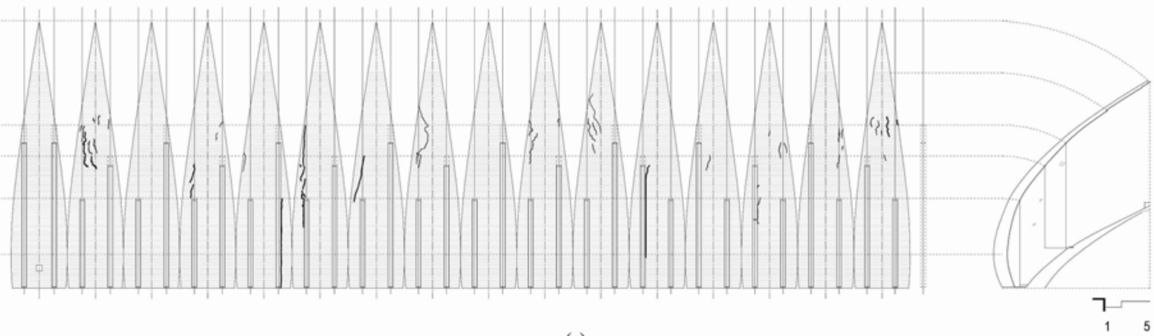


(c)

**Fig. 3.** (a) The restraint crack and the tie beams strengthening of 1932 for the South eyvan's semi-dome, and (b) a serious vertical crack on the sidewall of the eyvan, images by Ali T. Dinani; (c) the crack pattern of the outer dome: distribution of the cracks in the intersection of the stiffening walls and the bulbous dome are notably recorded on 24, August 2016, Reprinted from Dinani 2019, © Inter-Esse Studio.

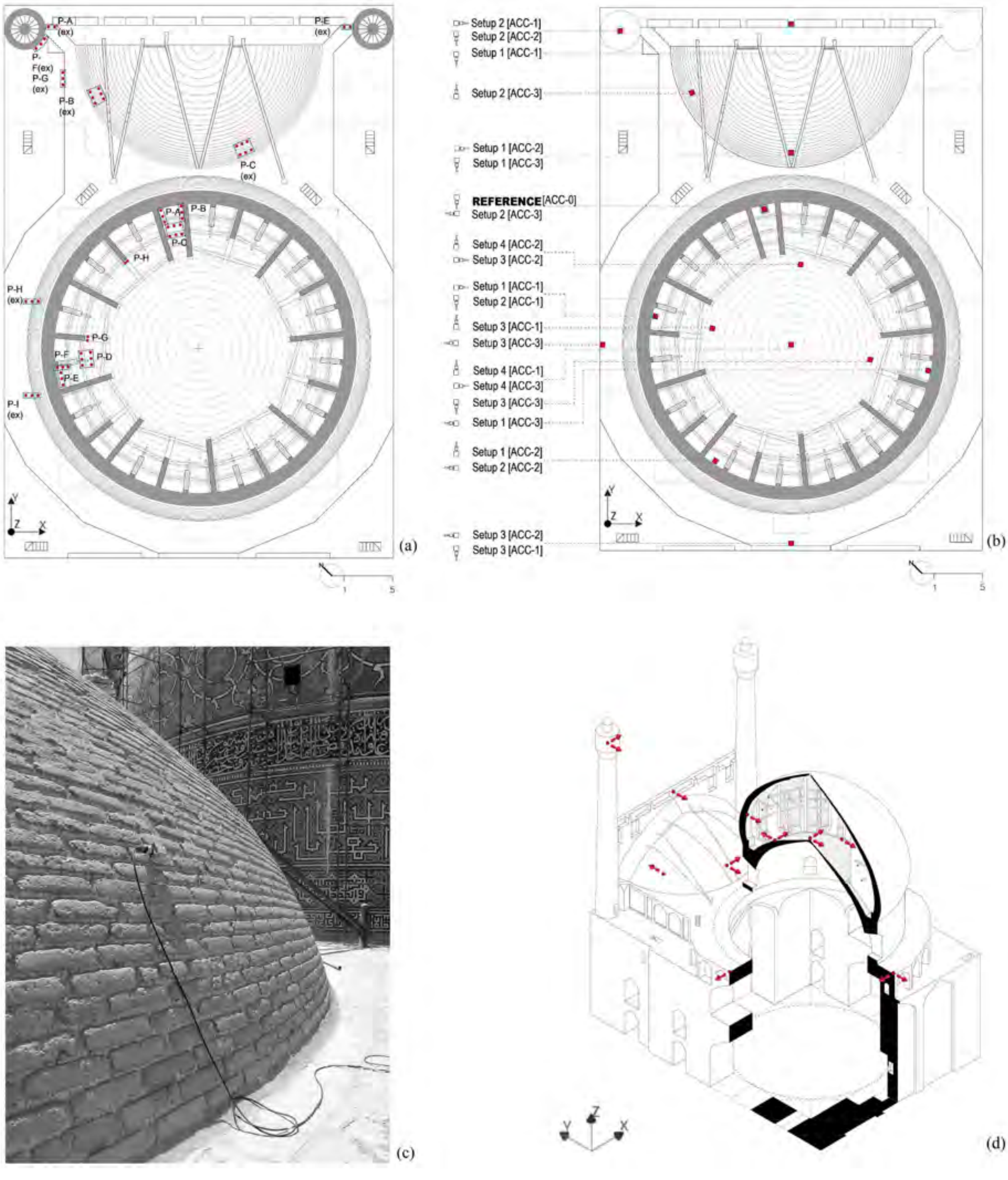


**Fig. 4.** In situ NDT of dynamic identification and sonic tests: (a) location of the sonic tests inside the double dome and the exterior part (tests were carried out mostly in the Western part of the dome due to the safety reasons related to the conservation works occurring in the Eastern part); (b) disposition of accelerometers in the performed setups for dynamic identification tests; (c) mounted accelerometer in the adhesive wooden base placed on the semi-dome of the eyvan, image by Ali T. Dinani; and (d) axonometric section view with sensors' location and measuring directions with arrows.

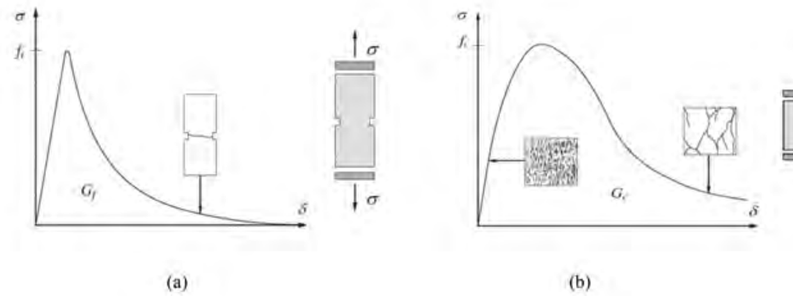

Fig. 5. Behavior of material under tensile (a) and compressive (b) loading and definition of fracture energy, Reprinted from Lourenco 1996.

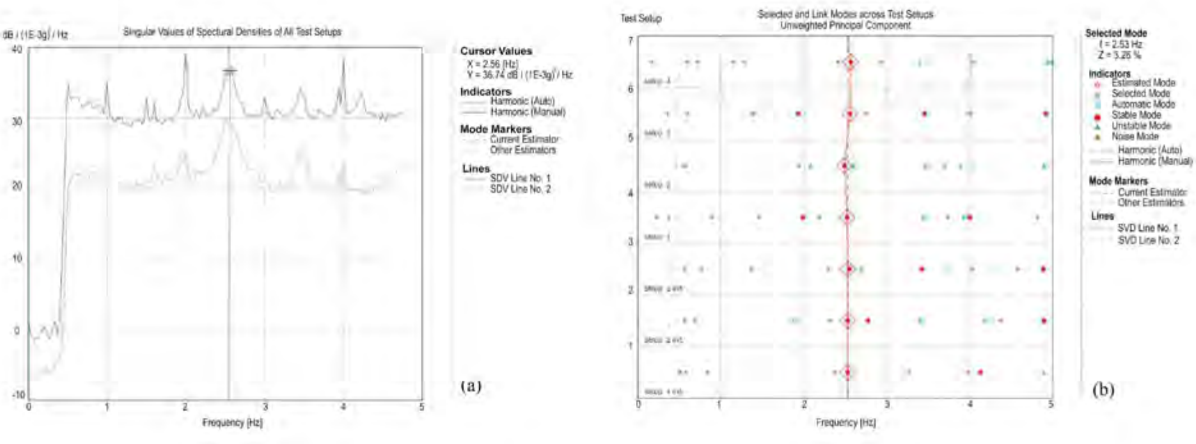

Fig. 6. Operational modal analysis: (a) Frequency domain techniques EFDD, with singular value of spectral densities of all setups; and (b) time domain technique SSI-UPC method, with selection and linking modes across all test setups.

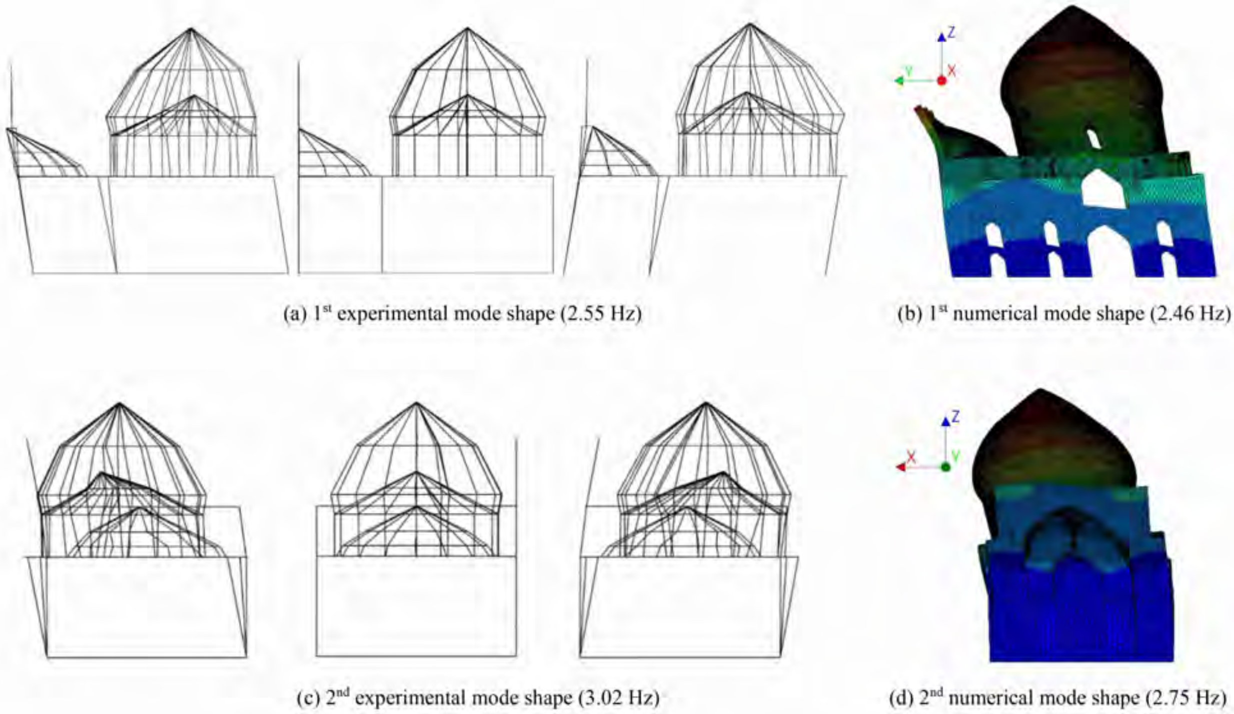

(a) 1st experimental mode shape (2.55 Hz)

(b) 1st numerical mode shape (2.46 Hz)

(c) 2nd experimental mode shape (3.02 Hz)

(d) 2nd numerical mode shape (2.75 Hz)

**Fig. 7.** Mode shapes of the first two modes, as taken from experimental dynamic tests (a) and (c) in comparison with the updated numerical model results (b) and (d).

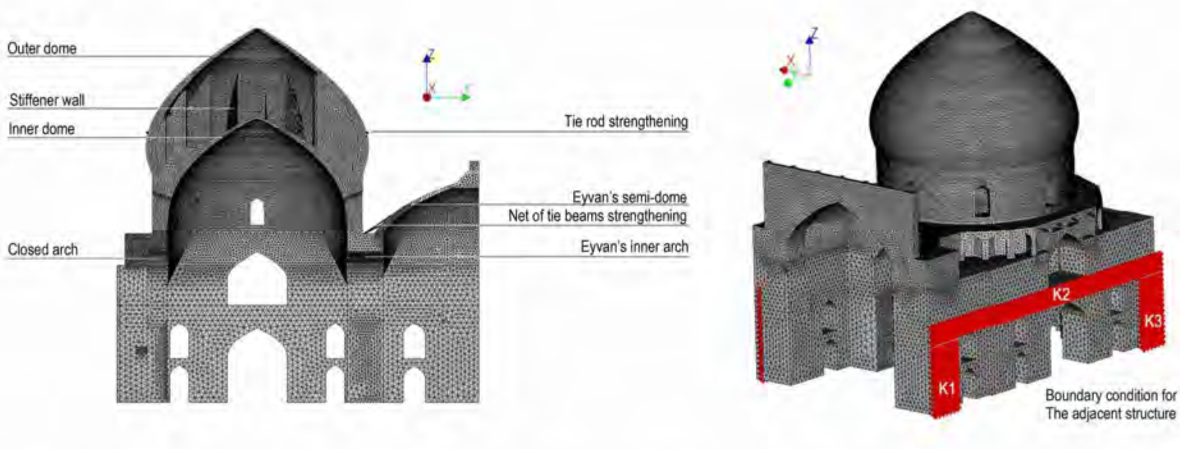


**Fig. 8.** Finite element model and boundary conditions considered simulating the adjacent structure

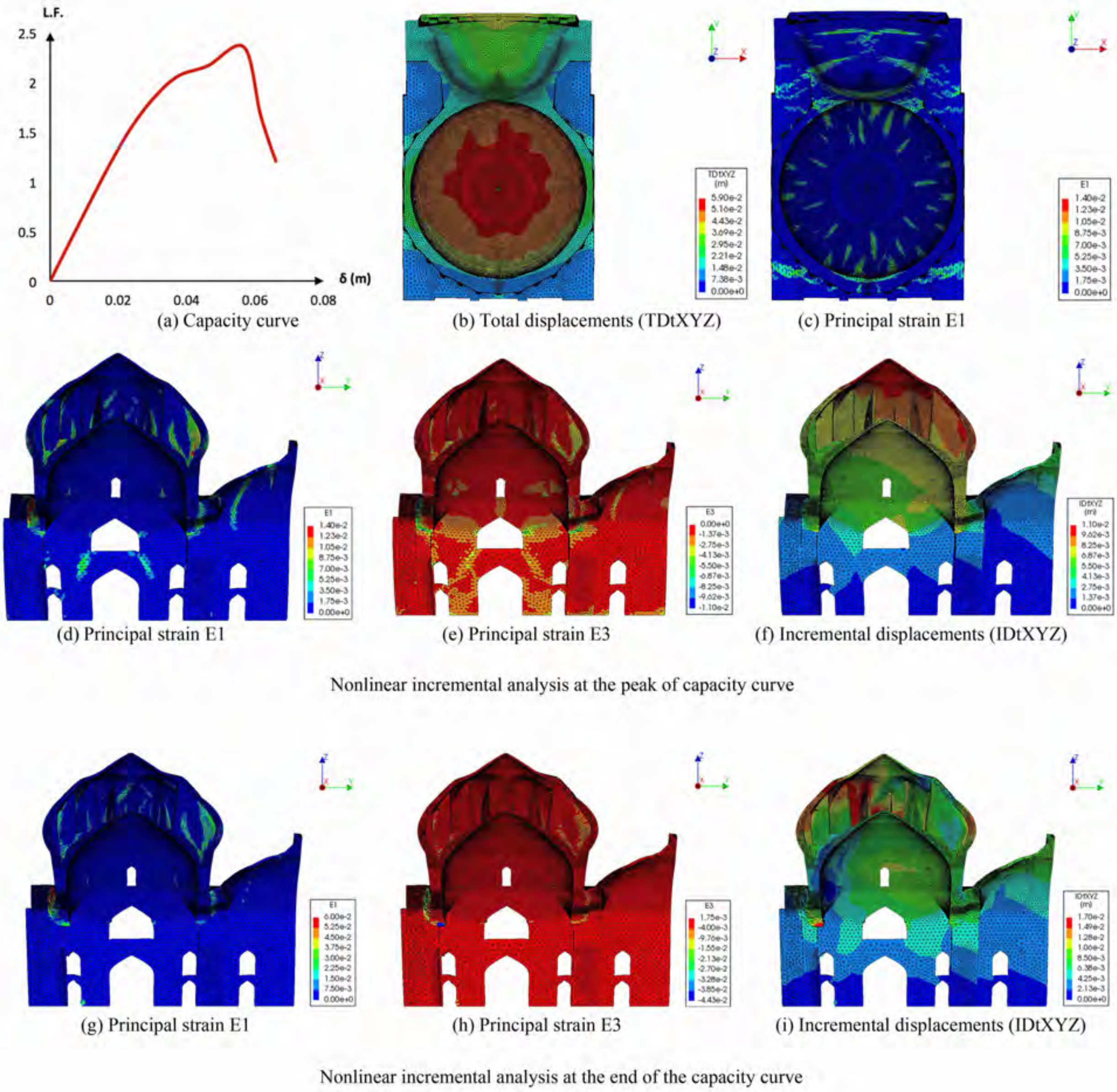


**Fig. 9.** Nonlinear incremental analysis due the vertical loading for the model with stiffening walls: (a) capacity curve for the control point at the top of the dome; damage patterns and displacement at the peak of capacity curve, load factor 2.35 (b), (c), (d), (e) and at the end of the capacity curve (f), (g) and (h).

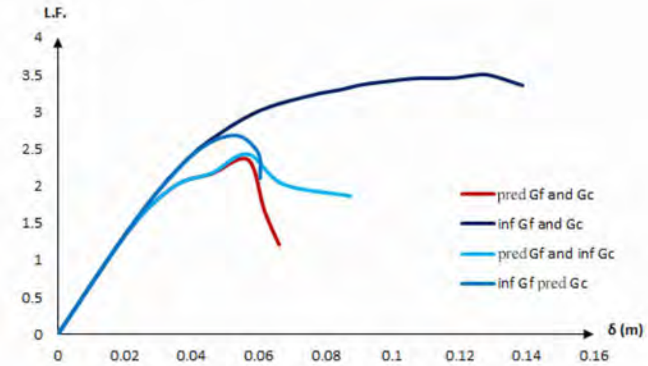

(a) Capacity curve

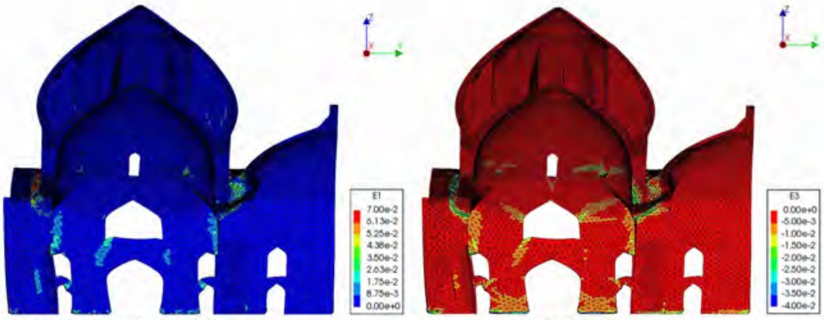
Principal total strain E1 Principal total strain E3

(b) infinite fracture energy in compression and tension

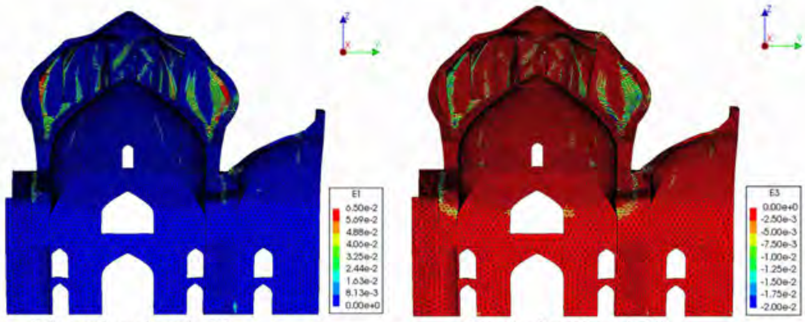
Principal total strain E1 Principal total strain E3

(c) predicted fracture energy in tension and infinite in compression

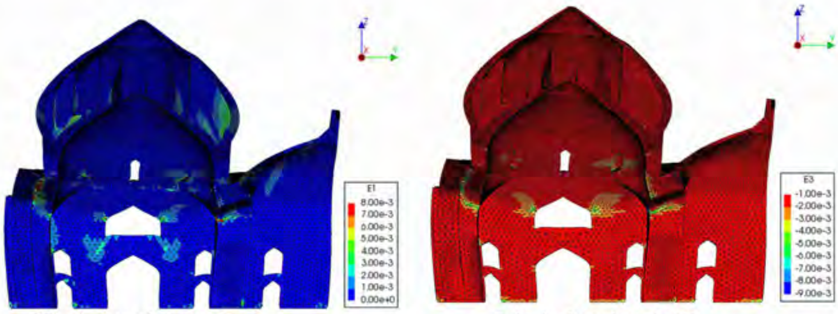
Principal total strain E1 Principal total strain E3

(d) predicted fracture energy in compression and infinite in tension

**Fig. 10.** Sensitivity analysis of fracture energy in tension and compression: (a) the capacity curve for the vertical loading with different scenarios; damage patterns for (a) infinite fracture energy in compression and tension at load factor 3.35; (b) predicted fracture energy in tension and infinite in compression at load factor 1.88; and (c) predicted fracture energy in compression and infinite in tension at load factor 2.66.

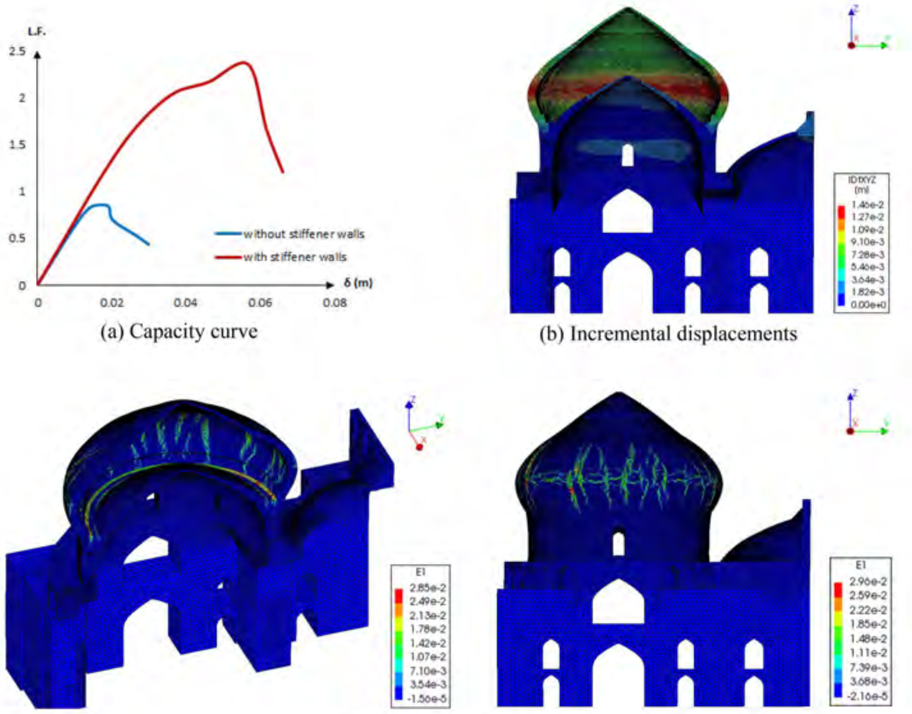


(a) Capacity curve

(b) Incremental displacements

(c) Principal strain E1

**Fig. 11.** Nonlinear incremental analysis due the vertical loading for the model without stiffening walls: (a) Capacity curve in comparison with the model including stiffening walls; (b) incremental displacements; and (c) principal strain E1 at about 50% of the self-weight and the end of the capacity curve.

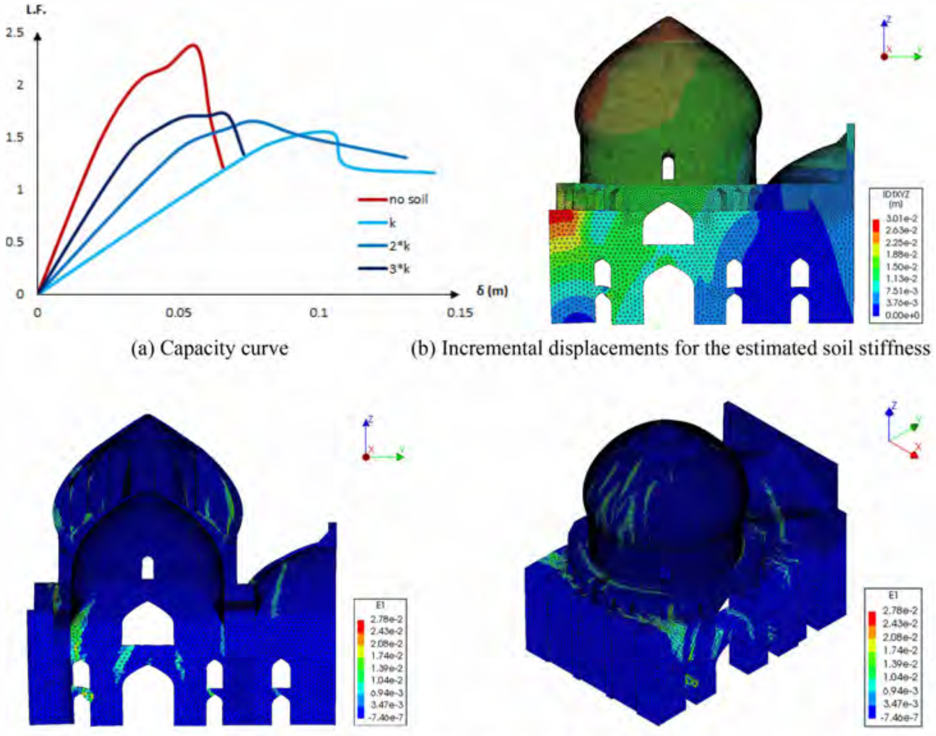


(a) Capacity curve

(b) Incremental displacements for the estimated soil stiffness

(c) Principal strain E1 for the estimated soil stiffness

**Fig. 12.** Nonlinear incremental analysis due the vertical loading for the model with soil influence: (a) capacity curve for the model considering the soil influence on the structure; (b) incremental displacements; and (c) principal strain E1 and damage pattern for the estimated soil stiffness at maximum load.

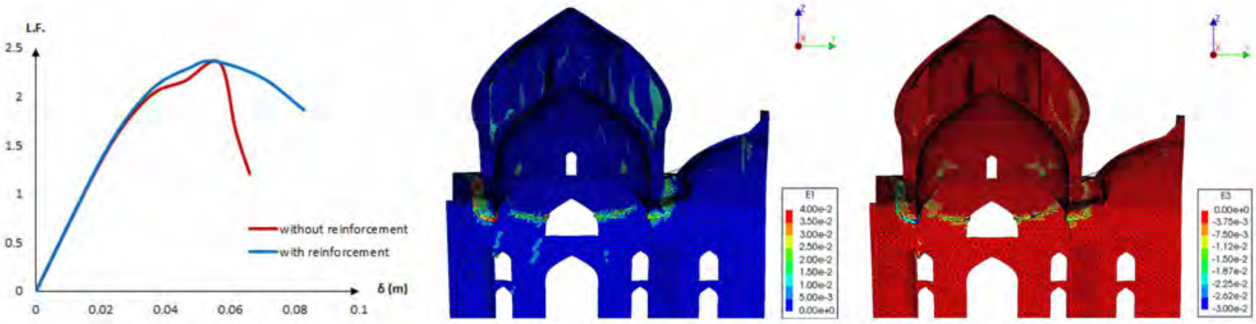


(a) Capacity curve (b) Principal total strain E1 (c) Principal total strain E3

**Fig. 13.** Nonlinear incremental analysis due to the vertical loading for the reinforced model: (a) capacity curve in comparison with unreinforced model; principal strain E1 (b) and E3 (c) after peak load.

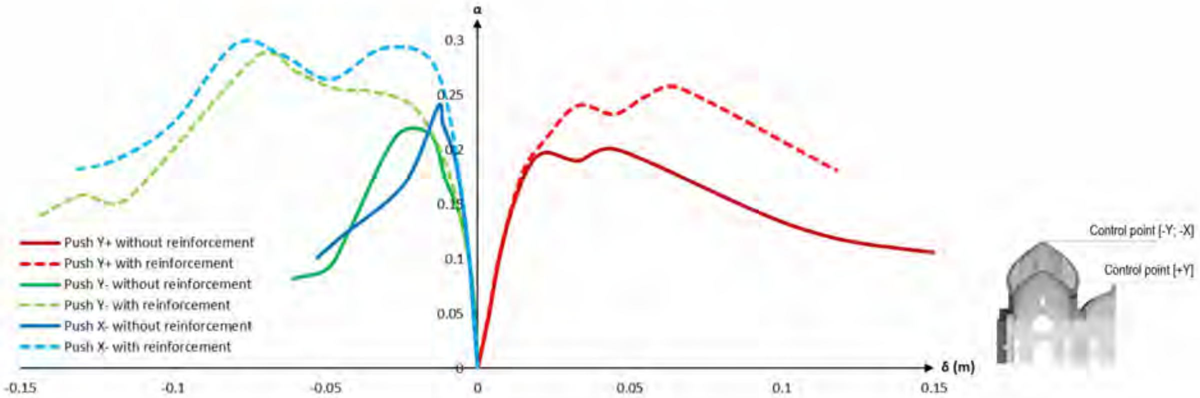


**Fig. 14.** Capacity curve for the pushover analysis for the model with and without reinforcement in the +Y (control point in the top of the eyvan), -Y and –X (control point in the top of the dome) directions.

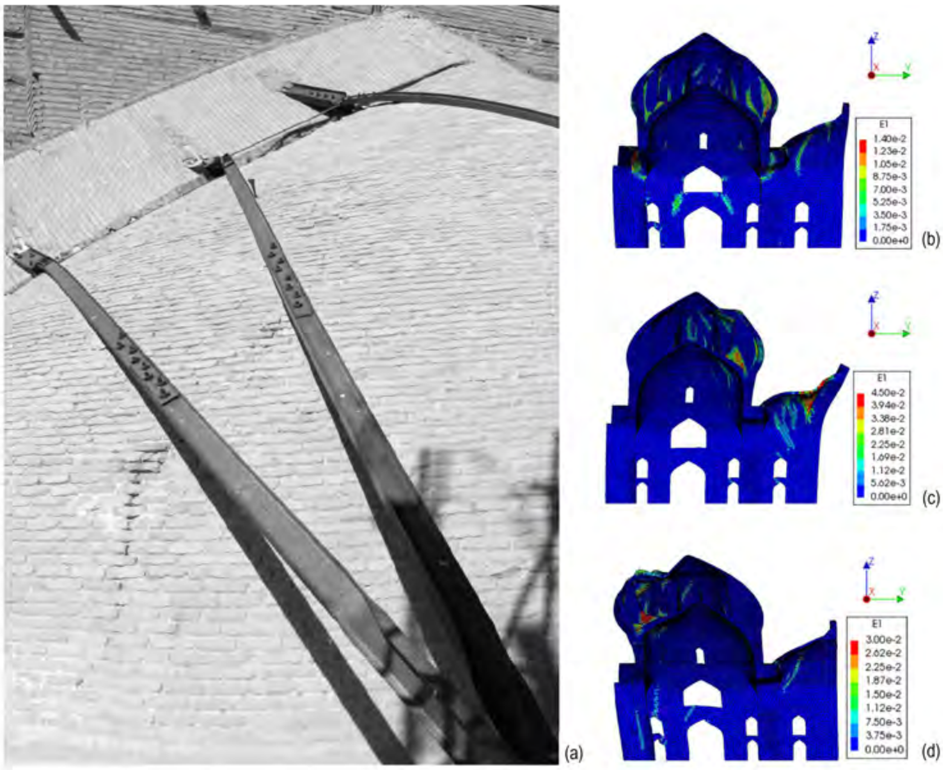


**Fig. 15.** Crack pattern correlation: (a) crack pattern in semi-dome of eyvan, image by Ali T. Dinani; Principal strain E1 and damage distribution due to the vertical loading (b) and horizontal loading in the +Y (c) and –Y (d) directions.

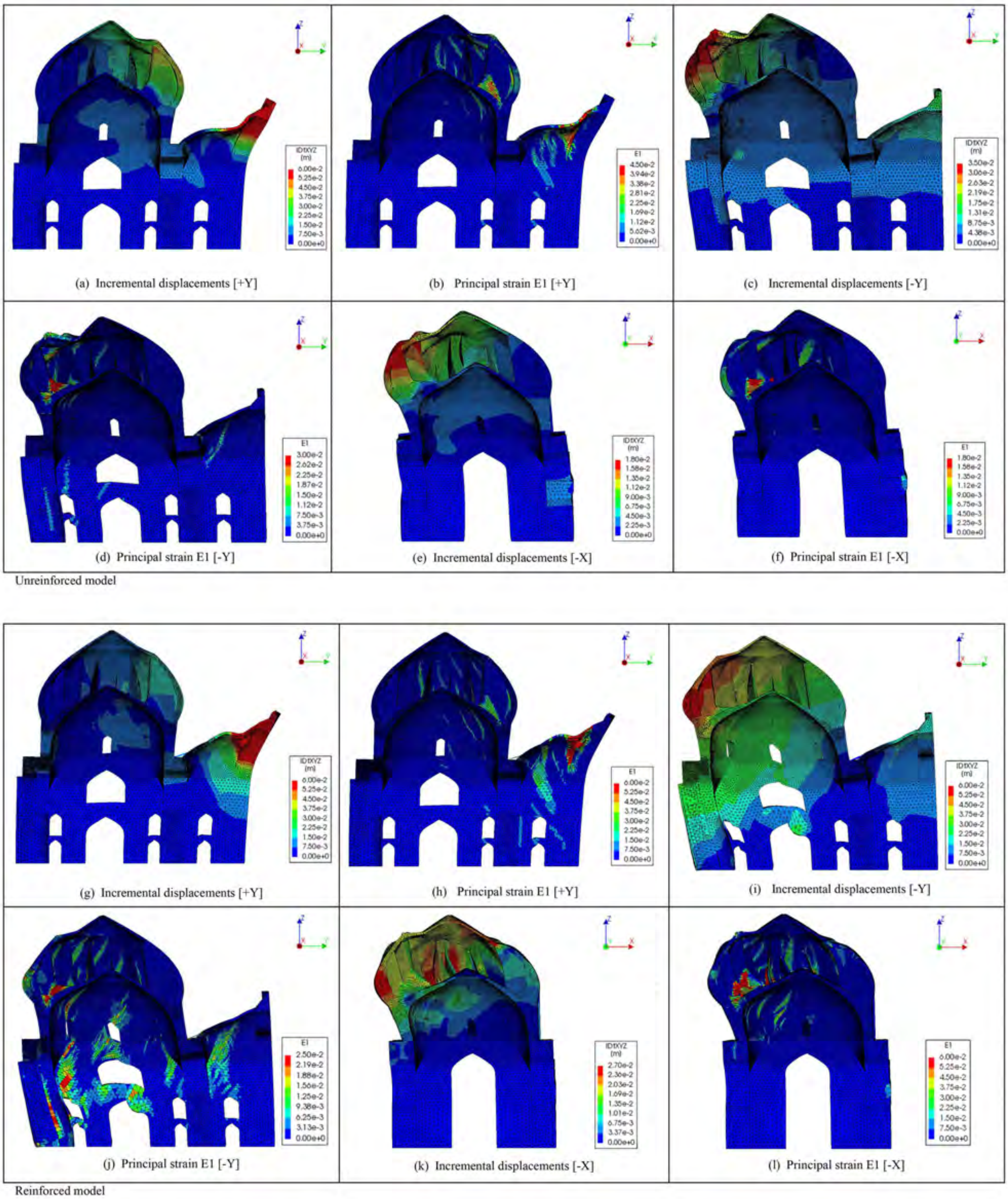


**Fig. 16.** Pushover analysis including incremental displacements and principal strain E1 at the post peak of the capacity curve for the unreinforced and reinforced model in the longitudinal directions +Y and -Y and transversal direction –X.